Cloud Microphysics of the Giant Planets

BARBARA E. CARLSON AND WILLIAM B. ROSSOW

NASA Goddard Space Flight Center, Institute for Space Studies, New York, New York

GLENN S. ORTON

Earth and Space Sciences Division, Jet Propulsion Laboratory, California Institute of Technology, Pasadena, California

(Manuscript received 5 October 1987, in final form 1 March 1988)

ABSTRACT

The predominant cloud microphysical processes for the atmospheres of the giant planets are determined by a comparison of their characteristic time constants. These results are an extension of the earlier microphysical modeling by Rossow to other atmospheres and by a more thorough exploration of thermal structure and compositional effects.

The NH_3 clouds on Jupiter and Saturn are found to be weakly precipitating systems, similar to the thicker cirrus clouds on Earth, while the H_2O clouds are much more massive than water clouds on Earth. The NH_4SH clouds are very tenuous on Jupiter and Saturn but may produce precipitation on Uranus and Neptune. The CH_4 and H_2O clouds on Uranus and Neptune are completely unlike any cloud on Earth, being 10–100 times more massive than the densest water clouds on Earth.

Horizontal contrasts in weakly precipitating systems, such as the NH_3 cloud on Jupiter may be muted and the vertical extent may be small in a weak dynamic regime or large in a multilayered haze complex, if stronger vertical motions exist. Denser precipitating cloud systems are expected to exhibit more horizontal structure with cumulus-style dynamics more likely due to larger latent heat effects. The massive CH_4 and H_2O clouds expected on Uranus and Neptune should dominate energy exchanges in the general circulation of these atmospheres.

1. Introduction

Gas and cloud opacities limit the depth to which remote sensing measurements can probe the tropospheres of the giant planets to the upper few bars. The first theoretical investigations of the vertical structure of these atmospheres used thermochemical equilibrium models (Lewis 1969; Weidenschilling and Lewis 1973) to predict the composition and location of the cloud layers based on the assumption that the atmospheric composition is roughly solar. Subsequent measurements by ground and spacecraft require changes in this assumption. More recent thermochemical equilibrium models for the atmospheres of Jupiter and Uranus (Carlson et al. 1987a,b) have been constructed using new thermal profile information and abundance determinations. These models have also been used to predict the vertical distributions of the photochemically stable compounds and the locations of the cloud bases. However, the predictions of the thermochemical models neglect the effects of atmospheric dynamics and cloud microphysical processes on cloud base location, cloud vertical distribution, and vertical distribution of condensible and soluble species. As a first step in the study of these effects, we examine the microphysical processes within the thermochemically predicted clouds layers for the giant planets to evaluate their characteristic time constants compared with dynamic and chemical time scales. This work is an extension of the earlier microphysical modeling of Rossow (1978, henceforth R78) to other atmospheres and by a more thorough exploration of thermal structure and compositional effects on the microphysical time constants. The objective, as in R78, is to find analogs for clouds in the atmospheres of the giant planets among the several types of cloud systems found on Earth. The analog can provide some insights into the potential complexity of the cloud vertical and horizontal structures.

We find that the microphysical characteristics of the clouds on Jupiter and Saturn are comparable to those of terrestrial stratus and cumulus clouds. The weakly precipitating systems are similar to stratus on Earth and are expected to exhibit little horizontal structure. The denser cloud systems are predicted to exhibit more spatial variability and cumulus-style dynamics influenced by latent heat effects. The very massive H_2O clouds on Uranus and Neptune reach conditions unlike anything on Earth.

Corresponding author address: Dr. Barbara E. Carlson, NASA Goddard Space Flight Center, Institute for Space Studies, 2880 Broadway, New York, NY 10025.

2. The model

The method introduced by Rossow (1978) for comparing the characteristic time scales for cloud processes is to estimate the rates of microphysical processes that determine the typical cloud particle size. The rationale for the time constant expressions is given in that paper; here, we emphasize the assumptions used and the interpretation of this type of analysis.

The key assumptions used to estimate the order of magnitude of the time constants are 1) that the cloud mass density is approximately equal to the vapor density of a condensible species at cloud base (lower limit on growth times), 2) that the cloud layer thickness is on the order of a scale height (upper limit on particle removal times), 3) that by assuming a well-mixed atmosphere the cloud base can be located using the thermodynamic formula for the saturation vapor pressure (lower limit on growth times), and 4) that the particle size distribution and the dependence of the processes on particle size are adequately represented by a *mass-weighted* mean particle size. These assumptions lead to estimates of upper limits on cloud particle sizes just above the base of a condensate cloud on Earth (R78). Cloud mass densities and layer thicknesses are typically smaller than assumed in this procedure, but only by factors ~3. As we show, changes of cloud mass density and thickness do not change estimated *cloud* particle sizes very much, but do change the sizes of precipitation particles. On Earth, cloud particle size and number density vary by factors of 2–4 among different clouds, whereas precipitation sizes can vary by more than an order of magnitude. These equations are also only meant to represent typical conditions; variations of the circulation regime will alter the specific properties of the clouds.

This type of analysis cannot determine the vertical structure of clouds (except by analogy) or the particle size and mass density near the cloud tops usually measured by satellites. These additional characteristics of condensate clouds depend on the interaction of dynamics and microphysics, which is beyond the scope of this analysis. Nevertheless, the analogy to better-observed clouds can provide an assessment of the importance of these cloud processes to the determination of the vertical structure of the clouds and the distribution of condensible (and soluble) chemical species.

a. Calculation of the microphysical time constants

The key processes to be considered are the condensation (evaporation) rate, coalescence and coagulation growth rates, and sedimentation rate (see R78, for definitions). The equations are derived as a function of mass-weighted mean particle size with the total cloud mass density fixed. The expressions are given for three regimes: Kn $\gg$ 1, Kn $\ll$ 1 and Re $\ll$ 1, and Kn $\ll$ 1 and Re $\gg$ 1. These represent the gas kinetic regime, the classical laminar flow regime, and the classical turbulent flow regime, respectively (R78). The Knudsen number, Kn = λ/a, is the ratio of the gas molecular mean free path, λ, and the cloud particle radius, a; while the Reynolds number, Re = $2a\rho v/\eta$, where gas density and dynamic viscosity are ρ and η, respectively, and v is the particle velocity. (The transition from laminar flow to turbulent flow regimes is expressed by an empirical formula at Re = 70. Equation 20 in R78 has a typographical error, a^2 should be a^3).

The condensation time is given by

$$\tau_{\text{cond}} = \rho_p a^2 (2x_s S_{\max} f\eta)^{-1} \quad (\text{Kn} \ll 1) \tag{1}$$

$$\tau_{\text{cond}} = (2\rho_p aRT/3x_s f\mu P S_{\max})(\pi\mu/2RT)^{1/2} \quad (\text{Kn} \gg 1) \tag{2}$$

where ρ_p is the bulk mass density of the cloud particle, x_s is the mass mixing ratio of the condensible gas at the cloud base (saturation level), $S_{\max} = 10^{-3}$ is the maximum supersaturation during condensation (see R78), f is a diffusion correction to account for the different molecular weights of the condensing gas and the atmosphere (which is important for the hydrogen atmospheres of the outer planets), R is the universal gas constant, μ is the mean molecular weight of the atmosphere, and P and T are the pressure and temperature of the atmosphere at cloud base. (Note that the use of $S_{\max} \sim 10^{-3}$ partially compensates for the overestimation of cloud mass density from the use of x_s). These formulae for condensation are obtained from the ratio of the vapor deposition rate, which is proportional to particle surface area, a^2, and the vapor supply rate, which is proportional to the vapor gradient (given by $S_{\max}$) times a diffusion velocity (proportional to the viscosity when Kn $\ll$ 1). This assumes a quasi-balance between the production of supersaturated conditions by the updraft and vapor consumption by particle growth; this is usually a good assumption if nucleation is moderately efficient (R78).

An upper limit to the evaporation rate for particles of radius, a, can be estimated using (1) or (2) by setting $S_{\max} = 1$; however, for conditions just below the cloud base 10^{-1} may be more typical. We assume that a cloud forms in a well-mixed atmosphere when the partial pressure of a species exceeds its saturation vapor pressure, a strictly thermodynamic quantity. Above the condensation level the vapor pressure of the species is set equal to its saturation value.

The coagulation time is given by the collision rate for particles in Brownian motion:

$$\tau_{\text{coag}} = \pi\rho_p a^3 N_0 \eta / x_s \mu P, \quad \text{Kn} \ll 1 \tag{3}$$

$$\tau_{\text{coag}} = (\pi\rho_p RT/3x_s\mu P)(\rho_p a^3/3kT)^{1/2}, \quad \text{Kn} \gg 1 \tag{4}$$

where N_0 is Avogadro's number and k is Boltzmann's constant. This form of these expressions is obtained by calculating the particle number density from

$$N = x_s(\mu P/RT)(4\pi\rho_p a^3/3)^{-1} \tag{5}$$

where the product of x_s and the atmospheric mass density, $(\mu P/RT)$, is the cloud mass density. This process is not important for the tropospheric condensate clouds considered here, but could play a role in determining the properties of the background aerosols, that could act as condensation nuclei. For the less dense stratospheric aerosols, nucleation processes may become so inefficient and condensation so slow, even with a buildup of large supersaturations, that coagulation may be the dominant growth process.

Coalescence time is given by the collision rate for cloud particles falling at slightly different speeds:

$$\tau_{\text{coal}} = (12\eta RT)(agx_s\mu P)^{-1}, \quad \text{Kn} \ll 1, \quad \text{Re} \ll 70 \quad (6)$$

$$\tau_{\text{coal}} = (8\rho_p aRT/15gx_s\mu P)^{1/2}, \quad \text{Kn} \ll 1, \quad \text{Re} \gg 70 \quad (7)$$

$$\tau_{\text{coal}} = (9/gx_s)(2RT/\pi\mu)^{1/2}, \quad \text{Kn} \gg 1 \quad (8)$$

where g is the acceleration of gravity. These expressions are obtained by assuming that the differences in sedimentation velocity, averaged over the particle size distribution, are about that of two particles with a mass ratio of 2 (R78). Coalescence is the only growth process that produces precipitation, which is defined as particles with sedimentation times much shorter than their evaporation times.

Coalescence growth is constrained to a limited size range by two effects: hydrodynamic effects of gas flow past a falling particle and collisional disruption (R78). The former inhibits collisions of small particles while the latter leads to an approximate upper limit on the size produced by coalescence where growth balances disruption. This limit applies to the average size of liquid droplets; however, the broad size distribution produced creates the larger, precipitation-sized, droplets. These two size limits on coalescence are given by

$$a < (9\eta)(2\rho_p v)^{-1} \quad (9)$$

$$a < (6\sigma)(\rho_p v^2)^{-1}, \quad \text{liquid droplets only} \quad (10)$$

where σ is the surface energy for the liquid. For solid condensates the sticking efficiency may be much less than unity, leading to much slower coalescence growth. The production of snow on Earth suggests that the sticking efficiency can be high and the disruption process inefficient for some solids.

The sedimentation time is the time required for the cloud particle to fall one scale height; for layered clouds the relevant time scale can be about a factor of 3–10 smaller than that given by

$$\tau_{\text{fall}} = (9H\eta)(2\rho_p ga^2)^{-1}, \quad \text{Kn} \ll 1, \text{Re} \ll 70 \quad (11)$$

$$\tau_{\text{fall}} = (3\mu P/4\rho_p agRT)^{1/2}H, \quad \text{Kn} \ll 1, \text{Re} \gg 70 \quad (12)$$

$$\tau_{\text{fall}} = (27\mu P/8\rho_p ga)(2RT/\pi\mu)^{1/2}H, \quad \text{Kn} \gg 1 \quad (13)$$

where the distance fallen is assumed to be $H = RT/\mu g$, the scale height.

b. Location of the cloud base

The dominant cloud-forming species in the atmospheres of the giant planets are expected to be CH_4, NH_3, H_2S, NH_4SH and H_2O. To determine the vapor pressure of species i in equilibrium with the condensed phase we use Raoult's Law

$$P_i = Kx_i \quad (14)$$

where P_i is the saturation vapor pressure in bars of species i, K is the equilibrium coefficient and x_i is the mole fraction. For the condensates considered here x_i is unity. The equilibrium coefficient is calculated from

$$\ln K = \Delta G/RT \quad (15)$$

where ΔG is the change in Gibbs free energy for the forward reaction, R the gas constant and T the temperature in Kelvin. The reactions and the associated thermodynamic data for H_2O liquid and solid, NH_3 solid, and NH_4SH solid are summarized in Table 1.

For some species adequate thermodynamic data are unavailable for Eq. (14); for these species we use empirical fits to the measured saturation vapor pressures. In all of these expressions the vapor pressure is in bars and the temperature in Kelvin. The saturation vapor pressure of NH_3 above the liquid (International Critical Tables, 1928) for $195 < T < 343$ K is

$$\log P_{NH_3} = 27.3816 - (1914.9569/T) - 8.4598324 \log T + 2.39309 \times 10^{-3}T + 2.955214 \times 10^{-6}T^2 \quad (16)$$

TABLE 1. The thermodynamic data at 298.15 K for the reactions used in the model. The data have been compiled from the Handbook of Chemistry and Physics (1983), International Critical Tables (1928), Kelley (1962), Kelley and King (1961), Wagman et al. (1968) and the JANAF Thermochemical Tables (1971).

Reaction	ΔH (kJ mol^{-1})	ΔG (kJ mol^{-1})	ΔS (J mol-K^{-1})
$H_2O(g) \Rightarrow H_2O(1)$	−45.00	−8.57	−122.20
$H_2O(g) \Rightarrow H_2O(s)$	−51.25	−7.97	−145.17
$NH_3(g) \Rightarrow NH_3(s)$	−31.67	9.86	−139.29
$NH_3(g) + H_2S(g) \Rightarrow NH_4SH(s)$	−89.97	−0.38	−282.45
$H_2S(g) \Rightarrow H_2S(s)$		see text	
$CH_4(g) \Rightarrow CH_4(1)$		see text	
$CH_4(g) \Rightarrow CH_4(s)$		see text	

while for the region $323 < T < 405.9$ K

$$\log P_{NH_3} = 5.056 - (T_c - T)[2.9771 - 1.4924 \times 10^{-3}(T_c - T) + 1.36142 \times 10^{-5}(T_c - T)^2 - 5.47919 \times 10^{-8}(T_c - T)^3]/T \quad (17)$$

where $T_c = 406$ is preferred. Equation (14) and the constants in Table 1 are used for NH_3 solid.

Following the *Handbook of Chemistry and Physics* (1983) the expression for the vapor pressure of CH_4 above the liquid in the range $99 < T < 110$ K is

$$\log P_{CH_4} = (-444.838/T) + 3.9875 \quad (18)$$

while the saturation vapor pressure of CH_4 above the solid (Ziegler 1959) in the range $50 < T < 90$ K is

$$\log P_{CH_4} = 4.820302 - 532.20/(T + 1.842) \quad (19)$$

The saturation vapor pressure of H_2S above the liquid (Giauque and Blue 1936) for $187.6 < T < 213.2$ K is

$$\log P_{H_2S} = -1145/T + 5.07226 - 0.00322T \quad (20)$$

and the vapor pressure above the solid in the range $164.90 < T < 187.7$ (Giauque and Blue 1936) is given by

$$\log P_{H_2S} = -1329/T + 7.41068 - 0.0051263T \quad (21)$$

These formulas and their application to temperatures beyond the indicated ranges have been verified with measured vapor pressures. Based on these comparisons, we estimate that the measured uncertainties in the thermodynamic data produce uncertainties in the cloud base pressures of less than 5% (Carlson et al. 1987a). Larger uncertainties exist in the case of H_2S because solid state transitions occur in the region 103–105 K and 121–123 K (Giauque and Blue 1936). These transitions alter the enthalpy of the solid and hence the vapor pressure.

Using the measured values for the entropy and enthalpy given in the *JANAF Thermochemical Tables* (1971) for gas and liquid N_2H_4, along with the heats of fusion and vaporization measured by Scott et al. (1949), we calculate the saturation vapor pressure for the gas above N_2H_4 solid from the equilibrium constant for the reaction

$$N_2H_4(g) \rightleftharpoons N_2H_4(s) \quad (22)$$

TABLE 2. Saturation vapor pressure formulae for the hydrocarbons.

Species	Formula
C_2H_2	$(-0.2185 \times 4665.8/T) + 5.20974$
C_2H_4	$(-0.2185 \times 3453.7/T) + 4.42311$
C_2H_6	$(-0.2185 \times 3739.5/T) + 4.402163$
C_3H_8	$(-0.2185 \times 4550/T) + 4.3418$

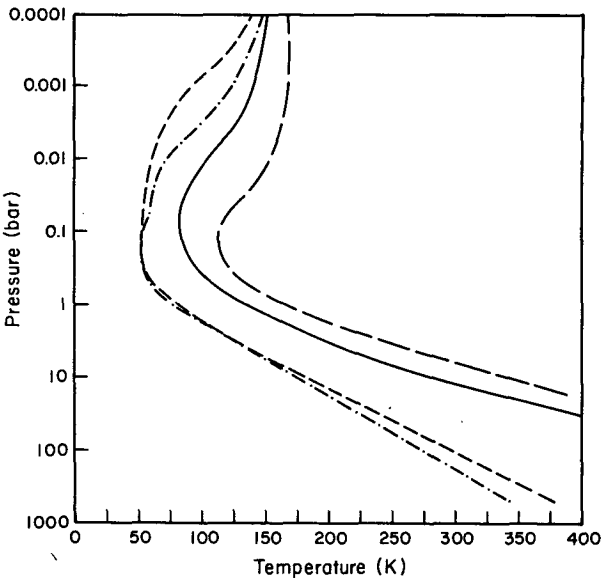

FIG. 1. A comparison of the pressure–temperature profiles for the giant planets used in our cloud models: for Jupiter (Orton 1981; long dashes), Saturn (solid line), Uranus (Orton et al. 1986; short dashes) and Neptune (Orton et al. 1986; dash-dot).

This may be expressed as a function of temperature by Eq. (15).

The formulae used to calculate the saturation vapor pressures for some of the photochemically produced hydrocarbons [e.g., acetylene (C_2H_2), ethane (C_2H_6), ethylene (C_2H_4), and propane (C_3H_8)] are taken from Ziegler (1959) and summarized in Table 2.

c. *Calculation procedure*

The pressure, temperature, dynamic viscosity (function of composition and temperature) and gas abundances are specified for each atmospheric level. For Jupiter, we use the P–T profile determined by (Orton 1981). This profile was based on a mean of the Voyager Radio Subsystem (RSS) occultation experiment results for the neutral atmosphere (Lindal et al. 1981) using the bulk composition determined by Gautier et al. (1981). A similar procedure was employed for Saturn using the *Voyager* RSS (Lindal et al. 1985), consistent with the composition assumed by Conrath et al. (1984). For Uranus and Neptune the profiles were determined from the results of Orton et al. (1986). These P–T profiles are shown in Fig. 1.

Finally, we must specify the remaining planet-specific variables. The values used for the gravitational acceleration g (Allison and Travis 1986) are given in Table 3. We assume atmospheric gas abundances consistent with recent measurements and in the absence of data assume solar abundances. The mixing ratios for the various condensates are given in Table 4. Since some elements, particularly C, have been observed or suggested to be present in supersolar abundance; we

TABLE 3. Values of the gravitational acceleration g used in our model.

Planet	g (cm s^{-1})
Jupiter	2260
Saturn	870
Uranus	875
Neptune	1090

also consider the consequences of increasing the mass densities of the clouds.

3. Results

Graphs of the microphysical time constants (Figs. 2–5 and 7–10) show their variation with mean particle radius in a constant mass cloud. Since the collisional growth processes conserve particle mass, the curves representing τ_{coag} and τ_{coal} are approximate evolutionary tracks for the particle radius in these clouds. The condensation process does not conserve particle mass, therefore the curve τ_{cond} is not an evolutionary track. This curve instead represents the growth time as a function of particle size and can be used to approximate the time required by a cloud to attain a particular mean particle size by integrating from smaller to larger size. Since the growth time is a strong function of particle size, the time to reach a particular size is only slightly longer than the growth time at that size, given by the τ_{cond} curves. More typical values near cloud base can also be estimated by reducing both cloud mass density and layer thickness by factors comparable to those observed for Earth under quiescent conditions, namely by a factor of 3 each.

TABLE 4. Values used for the gas abundances in the atmospheres of the giant planets. For reference the solar abundances of CH_4 and NH_3 are 8.35×10^{-4} and 1.74×10^{-4}, respectively.

	Jupiter	
NH_3	$(1.78 \pm 0.89) \times 10^{-4}$	Kunde et al. (1982)
H_2S	3.76×10^{-5}	solar; Cameron (1982)
H_2O	1.38×10^{-3}	solar; Cameron (1982)
	Saturn	
NH_3	$(0.5 - 2.0) \times 10^{-4}$	Courtin et al. (1984)
H_2S	3.76×10^{-5}	solar; Cameron (1982)
H_2O	1.38×10^{-3}	solar; Cameron (1982)
	Uranus	
CH_4	2.0×10^{-2}	Tyler et al. (1986)
NH_3	1.74×10^{-4}	solar; Cameron (1982)
H_2S	3.76×10^{-5}	solar; Cameron (1982)
H_2O	1.38×10^{-3}	solar; Cameron (1982)
	Neptune	
CH_4	2.0×10^{-2}	Bergstralh and Neff (1983)
NH_3	1.74×10^{-4}	solar; Cameron (1982)
H_2S	3.76×10^{-5}	solar; Cameron (1982)
H_2O	1.38×10^{-3}	solar; Cameron (1982)

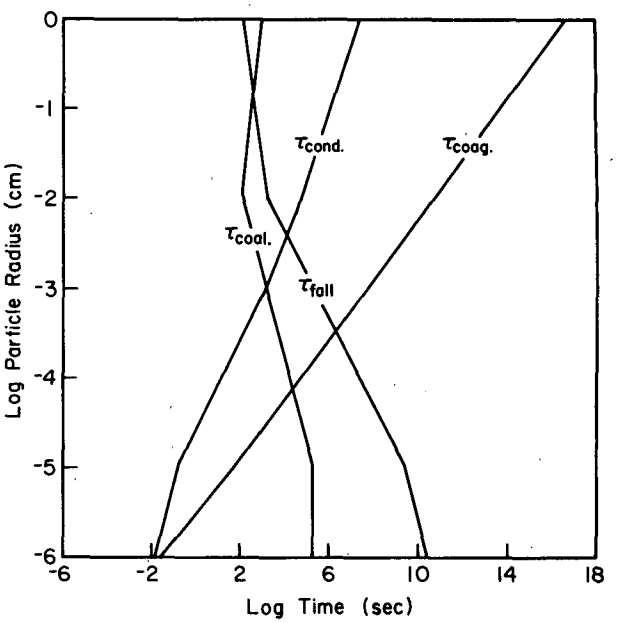

FIG. 2. The variation of the microphysical time constants with mean particle radius for an NH_3 cloud on Jupiter, an example of the relations in a weakly precipitating system.

These size estimates refer to the mass-weighted mean of the whole population, including any precipitation. In a precipitating cloud this size can be very large. The larger particles are neither long lived nor efficient scatterers of radiation; hence the "observed cloud" particles can represent a residual population with sizes near the transition from condensation to coalescence growth,

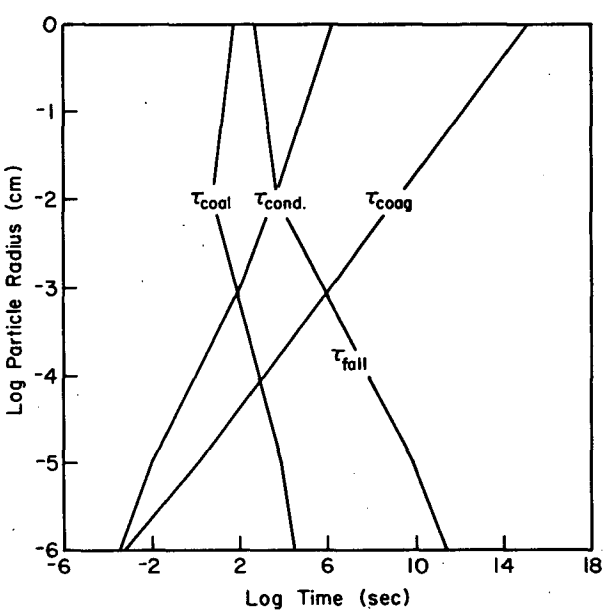

FIG. 3. The variation of the microphysical time constants for a solar abundance H_2O cloud on Jupiter, an example of a moderately precipitating system.

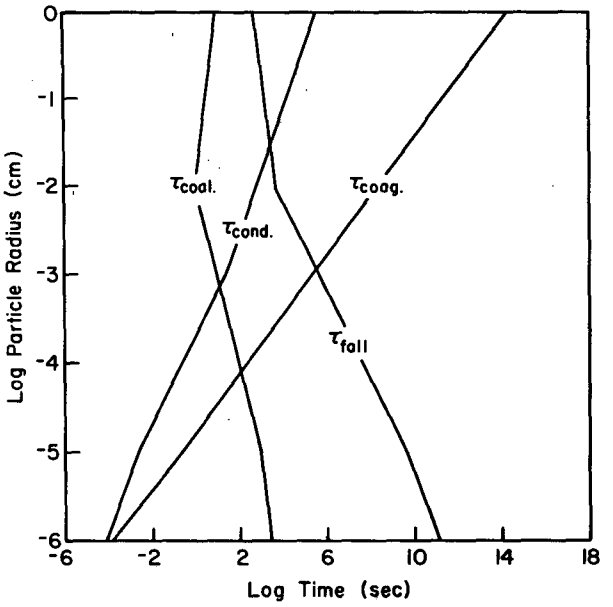

FIG. 4. The variation of the microphysical time constants in a CH_4 cloud on Uranus, an example of a heavily precipitating system.

typically about 10 μm, which is a "bottle-neck" in the evolution of the particles from condensation nuclei (CCN) to precipitation-sized particles. These graphs can be used to obtain an upper limit on particle size by finding a balance between growth and removal processes.

We illustrate the range of conditions encountered for tropospheric clouds by describing the model results for the NH_3 and H_2O clouds on Jupiter and the CH_4 and H_2O clouds on Uranus. The clouds produced by varying assumed temperatures and abundances, as well as by other substances, are either similar to one of these clouds or intermediate between them (see Table 5).

a. Non- and weakly precipitating clouds

An example of this cloud type is the NH_3 cloud on Jupiter. Clouds in this category are characterized by their relatively low mass density, typically less than 0.5 g m^{-3}. The mass density of the NH_3 cloud on Jupiter is ~0.16 g m^{-3}. These clouds are similar to denser cirrus clouds on Earth. There is little latent heat effect on the dynamics. Figure 2 shows the variation of the time constants with mean particle size. A slower condensation growth rate than used in R78, typical of direct vapor condensation to the solid phase, is used here because the equilibrium vapor pressure for the liquid and solid phases are found to be orders of magnitude apart. Condensation of the solid by way of a supercooled liquid phase occurs only when these two vapor pressures are closer in magnitude as is the case for H_2O on Earth.

From the figure it can be seen that the mean particle size increases by condensation until it reaches ~10 μm in times ~10^4 s (upper limit). At this point collisional growth processes take over and the particles may increase in size. With sedimentation limiting growth to a factor of 3 or less increase in the particle size, these clouds are described as weakly precipitating. The small mass density of the cloud and the fact that the Stokes limit for coalescence and the mean particle size are roughly equal implies that collisional growth processes will not be very efficient. In addition, the sticking efficiency of NH_3 ice crystals may be very low. Typical (lower) values of mass density and layer thickness would also reduce the role played by coalescence by increasing the condensation time and decreasing the sedimentation time. Thus, we expect that particle size near cloud base should be only ~10 μm. Particle sizes above the base will be smaller unless updrafts >1 m s^{-1} are present. Photochemical destruction of NH_3 in the upper troposphere on Jupiter would further deplete these upper level clouds since growth times are relatively large.

b. Moderately precipitating clouds

A typical cloud of this type is the water cloud on Jupiter. Figure 3 illustrates the variation of the microphysical time constants with particle size. The particle grows by condensation to ~10 μm in times <10^2 s. At this point collisional growth processes become important. The particle radius is slightly larger than the lower size limit on efficient coalescence. Since the cloud forms in the liquid phase at its base (Carlson et al. 1987a), collisional processes are effective. With typical values of mass density and layer thickness, the droplets

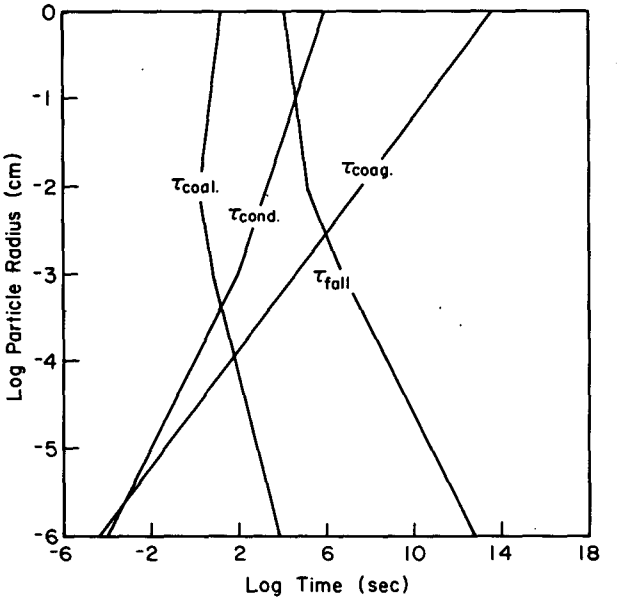

FIG. 5. The variation of the microphysical time constants with particle radius for the very dense H_2O cloud on Uranus, representing a novel cloud regime.

TABLE 5. Typical values for the cloud properties at the cloud *base*. For the different clouds T is the temperature in Kelvin, P is the pressure in bars, a is the mean radius in μm, N is the corresponding number density of cloud particles in cm^{-3}, τ is the time required to attain the mean particle size in seconds, σ is the particle column density in cm^{-2} and LWC is the mass density of the cloud in g m^{-3}.

Species	Parameter	Jupiter	Saturn	Uranus	Neptune
CH_4	T	—	—	79.6	80.6
	P	—	—	0.94	1.2
	a	—	—	5000	10 000
	N	—	—	1×10^{-4}	1×10^{-7}
	τ	—	—	300	200
	σ	—	—	8×10^{7}	1.6×10^{5}
	LWC	—	—	45	55
H_2S	T	—	116	124	124
	P	—	0.66	3.17	3.23
	a	—	20	300	300
	N	—	1	1×10^{-2}	1×10^{-2}
	τ	—	3×10^{4}	2×10^{3}	2×10^{3}
	σ	—	1×10^{5}	1×10^{8}	2×10^{8}
	LWC	—	0.09	0.4	0.4
NH_3	T	147	152	162	163
	P	0.66	1.39	6.74	7.62
	a	30	100	300	1000
	N	1.4	8×10^{-2}	4×10^{-2}	4×10^{-4}
	τ	2×10^{3}	2×10^{3}	3×10^{3}	3×10^{3}
	σ	6×10^{6}	3×10^{6}	2×10^{7}	1.5×10^{7}
	LWC	0.16	0.33	1.5	1.7
NH_4SH	T	209	215	233	237
	P	2.01	4.18	29.1	42.0
	a	100	500	1000	3000
	N	0.1	4×10^{-4}	3×10^{-4}	6×10^{-5}
	τ	2×10^{3}	3×10^{3}	10^{4}	10^{4}
	σ	3×10^{6}	3×10^{6}	3×10^{5}	4×10^{5}
	LWC	0.2	0.2	1	6
H_2O	T	274	284	328	348
	P	4.85	10.4	181	526
	a	60	100	200	300
	N	2	1	2	12
	τ	10^{2}	10^{2}	10^{2}	50
	σ	1×10^{6}	2×10^{6}	1×10^{7}	2×10^{8}
	LWC	5.3	11	170	450

reach $\sim$50 μm in about 100 s. The mass density of this cloud, $\sim$5 g m^{-3}, is larger than the lower limit for precipitation on Earth, $\sim$1 g m^{-3} and is comparable to very dense cumuliform clouds on Earth. Significant latent heat effects on dynamics are probable. The rapid formation of precipitation will significantly reduce the actual mass densities attained in these clouds, unless the updraft velocities are large.

The cloud systems discussed thus far are similar to water clouds on Earth and exhibit two key features: the size attained by the *cloud* particles in these condensate clouds is relatively insensitive to the cloud and atmospheric properties, while the onset and size of *precipitation* particles is more sensitive to the cloud mass density and vertical extent. In a nonprecipitating cloud ($\tau_{cond} = \tau_{fall} < \tau_{coal}$), the *cloud* particle size is determined by the balance between condensation growth and sedimentation. In a precipitating cloud ($\tau_{cond} = \tau_{coal} < \tau_{fall}$), the *cloud* particle size is set by a balance between condensation growth and the conversion of cloud particles to precipitation particles by coalescence. These balances lead to expressions for the cloud particle radius in terms of a^3 and a^4, by equating Eq. (1) to Eq. (11) and Eq. (6), respectively. However, the second balance does depend weakly on the cloud mass density and vertical extent; hence, denser, deeper clouds produce precipitation more readily. The size of *precipitation* particles is determined by the balance of coalescence growth and sedimentation; equating Eqs. (6) and (11) shows that the size is proportional to cloud mass density and vertical extent. Thus, while the values of the time constants are only order of magnitude estimates, the uncertainty of the *cloud* particle size is much lower.

c. *Heavily-precipitating clouds*

One example of this type of cloud is the methane cloud on Uranus. Figure 4 shows the variation of the

microphysical time constants with mean particle size. Condensation results in growth to sizes ~ 10 μm in times ~ 10 s. This cloud is much more massive than the H_2O clouds on Jupiter, with a cloud mass density of ~ 45 g m^{-3}, ten times that of large cumulonimbus clouds on Earth. The mean particle size attained through condensation growth processes is larger than the lower size limit for effective collisional growth. The size to which the particles grow through coalescence depends on the value assumed for the sticking efficiency. Since CH_4 forms as an ice near its freezing temperature, like water on Earth, the sticking efficiency may be near one, in which case, growth to 5000 μm is possible. As a lower limit, if we assume that the particles cannot grow through coalescence, growth by condensation to 100 μm still occurs before removal by sedimentation. In either case, large particles are produced in times $\sim 10^2$ s. Such rapid precipitation formation, again, implies that a significant depletion of the cloud mass occurs. If the mean vertical motions on Uranus are weak, much smaller mass densities might be the norm; however, the latent heat and density feedbacks on the dynamics may still produce local violent motions. If coalescence growth is effective, the *cloud* particle size would be ~ 10–30 μm; if, however, coalescence does not occur, then cloud particle sizes could be ~ 100 μm.

A more extreme example of this type of cloud is the H_2O cloud on Uranus. The variation of the microphysical time constants for this cloud are shown in Fig. 5. As a result of the large pressure encountered at the cloud base, collisional processes become important at much smaller particle sizes and sedimentation times are much slower. Collisional growth becomes faster than condensation growth at sizes ~ 5 μm; subsequent coalescence growth is limited by collisional disruption to a mean size of 200 μm. An additional limit on the size of liquid droplets is given by their stability against hydrodynamic pressures generated by falling; for Uranus conditions this limit is 1 cm in radius. This cloud produces precipitation sized particle in times $\sim 10^2$ s. The large mass density of the cloud, 170 g m^{-3}, is two orders of magnitude larger than those typically found on Earth; however, the rapidity of precipitation formation will significantly deplete the actual cloud, leaving *cloud* particle size of only ~ 10 μm.

Figure 5 shows that the sedimentation time constant is almost five orders of magnitude larger than the time required to attain collisional equilibrium. This remarkable situation implies that the cloud particle size distribution is determined solely by collisional processes, a condition likely to produce a very broad size distribution containing some very large particles. Such large cloud mass densities may not be sustained by the atmospheric motions, but even updrafts of 1 cm s^{-1} can produce heavily precipitating clouds. The very small microphysical time constants mean that the cloud properties immediately adjust to any changes in dynamics. The importance of latent heat exchanges and the drag exerted by large falling droplets suggest the probability of significant feedback effects on the general circulation; cloud processes may completely dominate vertical heat and momentum exchanges at these levels.

Table 5 summarizes the cloud properties on Jupiter, Saturn, Uranus and Neptune for "typical conditions" (i.e., mass density $\sim \frac{1}{3} x_s$ and vertical extent $\sim \frac{1}{3} H$) by displaying the bottom temperature, pressure, the mean particle radius, number density, mass density and the time required to attain this mean size. For clouds where coalescence is possible, the sticking efficiency is set to unity; the mean size attained is for the whole population (cloud plus precipitation). If precipitation is formed, the cloud particle size is about 10 μm for all cases. If coalescence is ineffective in the ice clouds, condensation growth still produces mean sizes of 30–100 μm. The particle sizes in the more massive H_2O clouds are limited by collisional disruption, whereas the sizes of "snowflakes" may not be limited. The microphysical balance attained in these clouds could vary with location.

Referring to Eqs. (1)–(13), we see that the condensation and sedimentation time constants are independent of cloud base pressure (as long as Kn $\ll 1$, Re $\ll 70$), whereas the coalescence growth time decreases at high pressures. Since large precipitation particles are formed in a solar abundance cloud, for which Re $\gg 70$, the sedimentation time actually increases as $P^{1/2}$ [Eq. (12)]; however, this does not affect the balance much since collisional disruption dominates the large-size part of the size distribution. These changes in the time constants mean that the deeper clouds initiate precipitation at smaller particle sizes in shorter times than the shallower clouds, suggesting increased horizontal contrast may be more characteristic of deeper, more massive clouds. Moving clouds upward inhibits precipitation, making the clouds more haze-like.

d. Uncertainties in the thermal structure

Uncertainty in the atmospheric temperature profile arises from 1) unknown, but real variations in the temperature structure as a function of location or time, 2) data uncertainties and systematic errors in the retrieval algorithm used to infer the temperature, and 3) extrapolation of the temperature profile to levels below the region where the temperatures are derived directly. Uncertainties from items 1) and 3) for the atmosphere of Jupiter are estimated, based on a comparison of the IRIS (Gautier et al. 1981) and Orton (1981) profiles, to be of order 5°–10°C. An error analysis pertinent to 2) above was performed by Orton (1981). He estimated a 1σ uncertainty of ± 2.3°C, considering 2°C uncertainty in the radio occultation results and 1.1°C uncertainty due to bulk compositional uncertainties. The uncertainties associated with the IRIS experiment are expected to be at or lower than this level, considering

the vertical smoothing of one-half to one or more scale heights implicit in the retrieval process.

For Saturn, real variations of temperature across the disk are likely to be larger than those found for Jupiter, at least in the stratosphere, owing to extremes of insolation to which the polar regions are subject. An error analysis similar to the one performed for Jupiter can be made by considering the 2.2 to 3.3°C uncertainty by which Lindal et al. (1985) characterize their temperatures (cf. their Fig. 4, right panel), irrespective of compositional uncertainties, between 100 mb and 1 bar. Independent compositional uncertainties are equivalent to about 1.3°C in temperature (Conrath et al. 1984), making the total 1σ uncertainty in the range 2.6–3.6°C.

Our calculations were made with the Orton et al. (1986) profile prior to the recovery of the temperature structure near the equator on Uranus from the *Voyager 2* Radio Science occultation experiment (Lindal et al. 1987). There are few significant differences between them for pressures of about 100 mb or greater. Even at pressures greater than the 2.3-bar maximum extent of the radio occultation experiment, our temperature is approximately consistent with their assumption of adiabatic conditions with a CH_4 volume mixing ratio of 2.3%. Our profile is cooler than theirs by about 10°C near 10 mb and warmer by as much as 20°C at pressures between 0.3 and 3 mb. Stratospheric temperature changes from seasonal variations of insolation are expected to be small (Wallace 1984), although *Voyager* IRIS observations detected variations of the zonal-mean temperature in the 60- to 200-mb range of 8°C (Flasar et al. 1987). One might expect similar differences between the profile we adopted for Neptune and the real one, particularly in the poorly constrained stratosphere. While Neptune's obliquity is similar to Saturn's, insolation-dependent stratospheric temperature variations are likely to be smaller, owing to longer radiative time constants for slightly colder conditions. As is the case for Uranus, dynamics may produce somewhat larger changes.

We investigate the effect of uncertainties in the thermal profile on our model results by considering the most extreme case using two different profiles for the atmosphere of Uranus. A comparison of the Orton et al. (1986) and the Appleby (1986) *P–T* profiles for the atmosphere of Uranus is shown in Fig. 6. Using a methane mixing ratio of 2.3×10^{-2}, corresponding to the Voyager-determined value (Lindal et al. 1987), we find that use of the colder Appleby profile shifts the cloud base to 1.7 bar from the 0.9 bar location obtained using the Orton et al. (1986) profile. The shift of the location of the cloud base to higher pressure changes the mass density of the cloud from ~40 g m^{-3} to 85 g m^{-3} but produces very little effect on the cloud properties because of the dominance of collisional growth.

Since the location of condensate clouds is essentially independent of pressure, small changes in the temperature profile serve only to shift the cloud location slightly. The weak dependence of the microphysical time constants on pressure means that the consequent changes in the cloud structure are due primarily to the change in cloud mass density with location. The dominance of collisional growth processes in all the tropospheric clouds makes the cloud relatively insensitive to such changes in cloud base location. Even the extreme case considered here does not exhibit much change in the cloud properties.

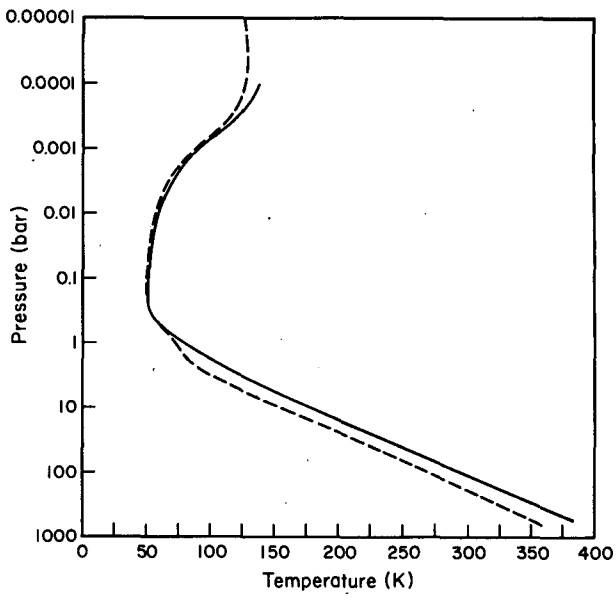

FIG. 6. A comparison of *P–T* profiles for the atmosphere of Uranus. The dashed line corresponds to radiative-convective model results (Appleby 1986) while the solid line is the profile determined by Orton et al. (1986).

e. Variation of abundance

Since the location of the clouds is controlled by attainment of vapor saturation with respect to the condensed phase, changing the assumed abundance shifts the cloud base in a similar fashion and with consequences similar to changing the temperature. Since the saturation vapor pressure is an exponential function of temperature, however, abundance changes must be very large, orders of magnitude, to shift the cloud base pressures significantly. We consider the consequences of several recent suggestions for altering the assumed abundances of the condensible species.

Observations of the NH_3 abundance on Jupiter have suggested a range of mixing ratios. Analyses of ground-based data (e.g., Sato and Hansen 1979) suggest NH_3 mixing ratios $(2.8 \pm 1.0) \times 10^{-4}$ at the 1 bar level. This value is consistent with the value $(1.78 \pm 0.89) \times 10^{-4}$ determined by Kunde et al. (1982) for the 1 bar level from their analysis of *Voyager* IRIS spectra from the North Equatorial Belt (NEB). A slightly larger value $(2.2 \pm 0.8) \times 10^{-4}$ was inferred by Lindal et al. (1981)

from their analysis of the *Voyager* RSS signal attenuation. Depleted NH_3 abundances have been inferred by de Pater and Massie (1985) and de Pater (1986) from observations of Jupiter at radio wavelengths. Their analysis suggests that the NH_3 abundance is depleted to $\sim 3 \times 10^{-5}$ in the region from 0.5 to 1.5 bar. At pressures larger than 2 bar, their analyses require an enhanced NH_3 abundance of 1.5–2 times solar.

Figure 7 shows a comparison between the microphysical time constants for two ammonia clouds formed with the upper and lower limits on the ammonia abundance at the 1 bar level determined by Kunde et al. (1982). The lower ammonia abundance, 8.9×10^{-5}, results in a thinner, non-precipitating cloud with a base at 0.6 bar (143 K). The mass density of this cloud is ~ 0.08 g m^{-3}. The upper limit on the ammonia abundance, 2.67×10^{-4}, produces a cloud that is marginally able to produce precipitation on time scales $\sim 10^4$ s. The cloud base is shifted to higher pressure, 0.7 bar (150 K). The mass density of this cloud is ~ 0.2 g m^{-3}. Both of these clouds resemble cirrus clouds on Earth. Although variations in dynamics may produce some precipitation, even if the cloud density is at the upper limit, these clouds are expected to be haze-like and exhibit more vertical than horizontal variations.

Recent determinations of the water abundance (Bjoraker et al. 1986; Kunde et al. 1982) suggest that the abundance of water on Jupiter may be substantially depleted with respect to solar values. Both of these investigations have suggested that the mixing ratio of water is $\sim 3 \times 10^{-5}$ near the 4 bar level. Taking this abundance as representative of the well-mixed water abundance, we find that a cloud forms at 2.67 bar (229 K). This cloud most likely forms in the ice phase, but the factor of 1.4 difference between the saturation vapor pressures of ice and liquid allows for the possibility that this cloud may form from supercooled liquid droplets, depending on atmospheric dynamics. The variation of the microphysical time constants with particle radius for this cloud are intermediate between those for the NH_3 cloud and H_2O cloud on Jupiter shown in Figs. 2 and 3. The mass density of this cloud is 3.2 g m^{-3}, still quite massive by Earth standards. The average particle size is ~ 10 μm. This cloud is moderately precipitating and similar to the cumulonimbus clouds on Earth.

The analyses of the 5-μm spectrum of Jupiter by Bjoraker et al. (1986) and Kunde et al. (1982) did not, however, include the presence of such dense clouds; they even differ by 2 bars in the pressure level at unit optical depth for a pure gas atmosphere due to differences in the boundary conditions and treatment of the sub-Lorentzian behavior of the far wings of the absorption lines. Abundances are assigned to a pressure level based on the opacities of gas only. If, as suggested by our microphysics results, cloud extinction is significant, the pressure associated with unit optical depth would be significantly reduced. A complete analysis, including the effects of the spectrally dependent absorption and scattering associated with NH_3 and H_2O

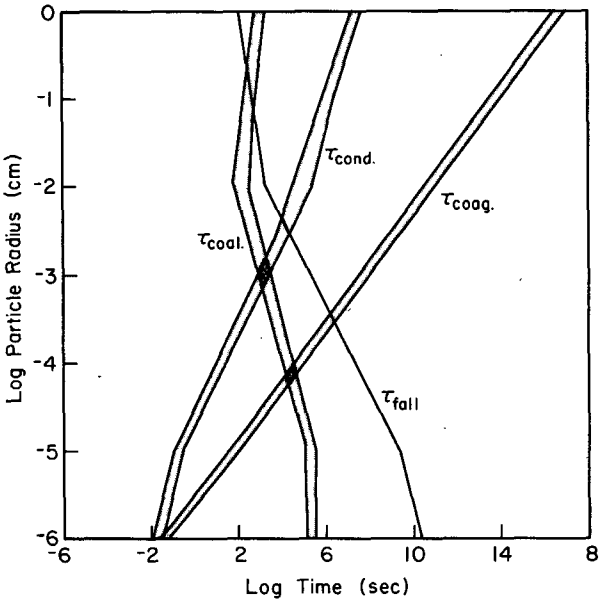

FIG. 7. An illustration of the effects of the variation of abundance on the microphysical time constants for the NH_3 cloud on Jupiter. The curves shown here correspond to the range of abundance as determined by Kunde et al. (1982). The lower limits for each time constant correspond to an NH_3 abundance of 2.7×10^{-4}, while the upper limits correspond to an abundance of 8.9×10^{-5}.

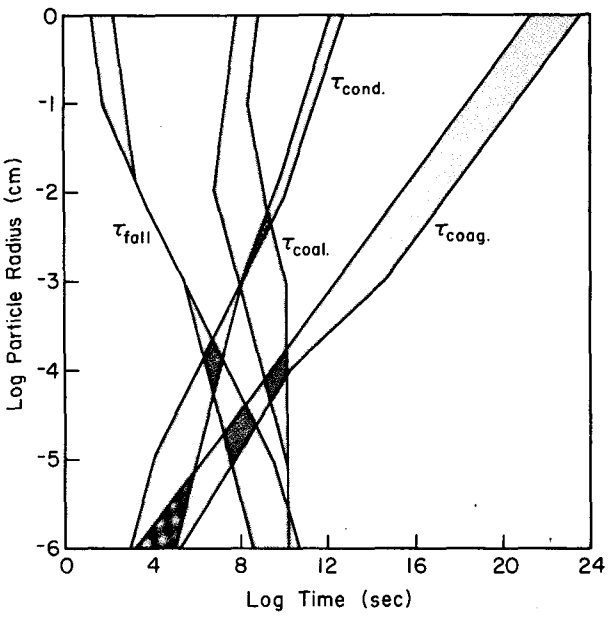

FIG. 8. An illustration of the range of variability in the microphysical time constants from the top (righthand curves except for τ_{fall}) to the bottom (lefthand curves except for τ_{fall}) of a hydrazine cloud that extends from the lower stratosphere to the upper troposphere on Jupiter.

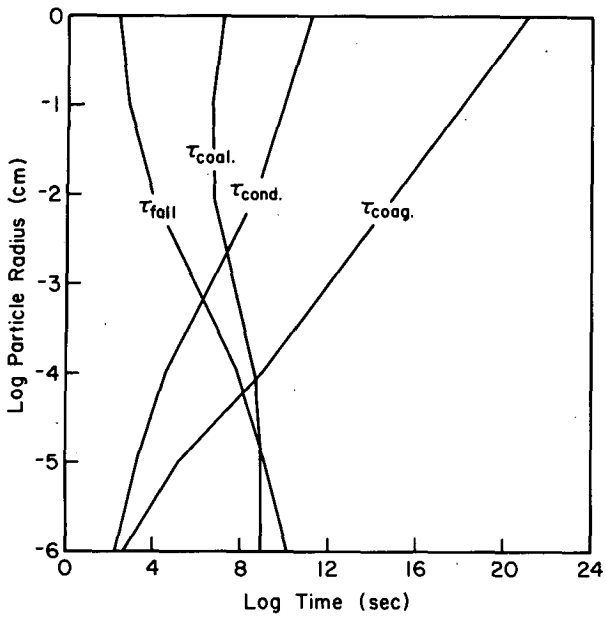

FIG. 9. Microphysical time constants for a stratospheric acetylene cloud on Saturn.

ice clouds, is required to obtain better measures of abundances at pressures greater than 2 bars.

Chemical processes may also alter the abundances of the cloud-forming species or produce new condensates. Results of thermochemical studies including the effects of aqueous chemical reactions (Carlson et al. 1987a,b) imply that chemical reactions within the atmospheres of the giant planets deplete the NH_3 abundance by 30%–40%. The effect of this depletion is to move the cloud base to lower pressure and decrease the extent of the cloud layer with only marginal changes to the cloud microphysics. The thermochemically inferred NH_3 abundances at the NH_3 cloud base are within the observational constraints.

f. Stratospheric clouds

Once a cloud has formed in the troposphere; the mixing ratio of the condensate will decrease exponentially with decreasing temperature following the saturation vapor profile. The interaction of atmospheric dynamics and precipitation can, in fact, produce an undersaturated layer above the main cloud formation level, as occurs in the Earth's upper troposphere; however, turbulent mixing will maintain the relative humidity at nearly 100% at upper levels where precipitation is no longer efficient. If mixing processes were to inject methane into the stratospheres of Uranus and Neptune, then subsequent downward motion could produce a cloud. A similar process has been suggested to explain the ice clouds in the polar stratosphere on Earth (McCormick et al. 1982). The injection of methane into the stratosphere of Neptune has been proposed as the mechanism responsible for the strongly inverted thermal profile (cf. Appleby 1986). The results of microphysical model calculations for Uranus and Neptune suggest that such an injection of CH_4 could produce a tenuous haze composed of submicron sized particles. The presence of such a cloud would interfere with remote sensing analyses, particularly thermal soundings, by creating an additional opacity source.

Strobel (1973) and Atreya et al. (1977) have suggested that the production of hydrazine, N_2H_4, from the *in situ* photochemical destruction of NH_3, may be a significant source of stratospheric aerosols on Jupiter. No ultraviolet absorption features due to NH_3 have been detected on Saturn (Caldwell 1977; Prinn et al. 1983) implying that only trace amounts of NH_3 are present in the Saturnian stratosphere. Thus NH_3 photochemistry is probably not an important source of stratospheric aerosols on Saturn. Deeper NH_3 cloud base pressures in the colder atmospheres of the remaining giant planets imply more efficient precipitation scavenging, making it unlikely that the products of NH_3 photolysis contribute to their stratospheric aerosol population (however, see Carlson et al. 1987b).

If photochemical production rates are enough to cause N_2H_4 vapor saturation in the stratosphere, then a cloud will form over the entire near-tropopause region. Under Jovian conditions, the low value of the saturation mixing ratio is consistent with the less than 1 ppb (part per billion) upper limit on the hydrazine abundance inferred from IUE data (Wagener et al. 1985). Figure 8 shows the range of the microphysical

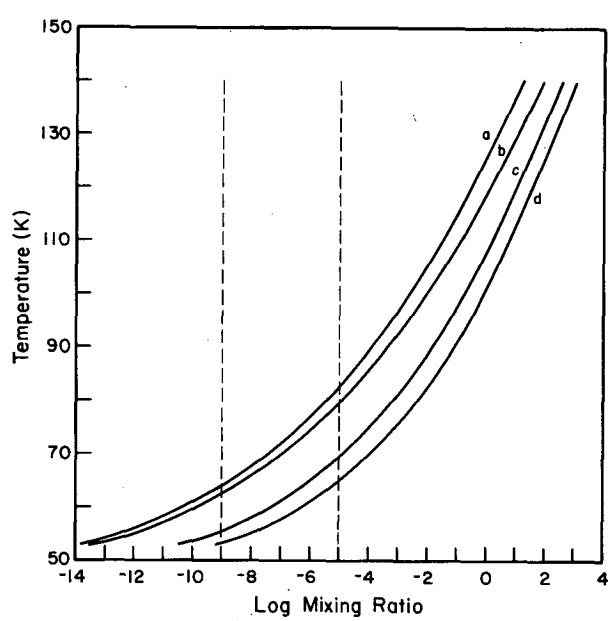

FIG. 10. A comparison of the saturation mixing ratio profiles versus temperature for propane (C_3H_8, curve a), acetylene (C_2H_2, curve b), ethane (C_2H_6, curve c) and ethylene (C_2H_4, curve d). The dashed lines indicate mixing ratios of 10^{-5} (the methane abundance at the tropopause) and 10^{-9} (lower limit for detection).

time constants from the top of an N_2H_4 cloud in the stratosphere ($P \sim 10$ mb) to the bottom in the upper troposphere ($P \sim 1000$ mb): the mean particle size attained varies from ~ 0.1–2 μm over about one scale height in the region of the tropopause. This size range in the stratosphere is consistent with that inferred from observations (West et al. 1986). Since NH_3 photolysis occurs throughout this same region, the actual variation of N_2H_4 aerosol production rate and particle size with altitude could be quite complex.

Since the condensation rate for low supersaturations is low, rapid photochemical production of N_2H_4 might maintain much higher supersaturations, as occurs for sulfuric acid on Earth (R78). This would produce larger particles; however, as with tropospheric clouds, the particle size at which condensation growth balances sedimentation is insensitive to the assumed cloud mass density, vertical extent, and assumed supersaturation [Eqs. (2) and (13)]. The photochemical model of Strobel (1973) and West et al. (1986) implies a large photochemical production rate of N_2H_4, but they argue that very large particles (>10 μm) are formed that leads to a removal of 99% of the N_2H_4 and leaves behind the tenuous, small particle haze inferred from the observations (West et al. 1986). Figure 8 shows that this sort of balance is not possible, since the only process that can produce a distinct separation of the condensing substance into a small and large size fraction is coalescence, which is not effective at these cloud mass densities. Thus, since the balance between condensation growth and sedimentation removal generally leads to a relatively narrow particle size distribution (R78), the larger particles produced, which still have sedimentation times of hours, would be observable. Not only is the observed cloud tenuous, but the upper limit on the vapor abundance precludes the supersaturations needed to produce such large particles ($S_{max} > 1000\%$).

The results of our analysis indicate that acetylene, C_2H_2, may condense in the stratospheres of some of the giant planets. While the abundance of C_2H_2 would have to increase by a factor of 10^4, from 10^{-8} to 10^{-4}, for C_2H_2 condensation to occur in the Jovian stratosphere, it is important to remember that these results correspond to global mean conditions. Horizontal temperature variation of order 10°C occur within the Jovian stratosphere (Lindal et al. 1981). Furthermore, as suggested by Caldwell et al. (1979) temporal variation in the stratospheric thermal structure may occur. Seasonal variations could actually be larger than 10°C for the polar regions at pressures of 10 mb or less (Bezanger et al. 1986). These temperature variations, coupled with latitudinal variations in the C_2H_2 abundance, may be large enough for saturation to occur. More detailed observations are required to explore this possibility fully.

The colder stratospheric temperature minimum on Saturn allows C_2H_2 to condense with observed abundances. Using the mixing ratio, 2.1×10^{-7}, for C_2H_2 determined by Courtin et al. (1984) from their analysis of the *Voyager* IRIS spectra, we find that a cloud forms near 0.06 bar. Unlike the situation for ethane (C_2H_6), where observational evidence suggests that the mixing ratio decreases dramatically below the 20–50 mb level, there is no strong observational evidence that the C_2H_2 abundance behaves similarly. Thus, although the condensation level is below the C_2H_6 abundance cutoff, acetylene condensation will occur provided the abundance is larger than 10^{-7} at the 0.06 bar level. Larger abundances of acetylene would shift this location to lower pressures because of the temperature inversion. A cloud at this location agrees with the location of the stratospheric haze layer determined by Tomasko and Doose (1984) and West et al. (1983) from their analysis of visible and ultraviolet data.

Figure 9 shows the time constants for a stratospheric acetylene cloud on Saturn. Since the abundance seems large enough for vapor condensation to predominate over coagulation, the growth of particles > 1 μm appears possible. Although the time required to grow a 1 μm sized particle is $\sim 10^4$–10^5 s, this is still much shorter than the time required to produce aerosols in Earth's or Venus' stratosphere (R78). If the photochemistry producing acetylene is more rapid than vapor condensation, then large particles (~ 3–6 μm) are possible, with a supersaturated layer nearly a scale height in thickness. Such large particles could account for the difficulties encountered in matching infrared and radio occultation results for the Southern Hemisphere (Conrath et al. 1984). A thinner production region or slower photochemical reaction rates would limit particle size to ~ 1 μm. The smaller particle sizes are preferred in the analysis of the *Pioneer* polarimetry and photometry (Tomasko and Doose 1984).

It is again important to remember that both the abundance of C_2H_2 and the thermal profile used correspond to global mean conditions. As shown by the *Voyager* IRIS results (cf. Fig. 3, Hanel et al. 1981), significant latitudinal variations in the stratospheric thermal structure occur. These latitudinal variations are coupled with or are the result of seasonal variations produced by Saturn's 27° obliquity (Carlson et al. 1980; Bezard and Gautier 1985). In light of this, acetylene clouds are likely to display a complex and temporally varying latitudinal structure; the latitudinal dependence of the acetylene abundance as determined by Courtin (1982) from his analysis of the *Voyager* IRIS spectra suggests that such variations do indeed occur.

Based on photochemical production rates, West et al. (1986) suggest the production of diphosphine (P_2H_2) from phosphine (PH_3) photolysis as the source of stratospheric aerosols on Saturn. The lack of vapor pressure curves as a function of temperature for P_2H_4 prevents us from including it in this analysis. We note, however, that the high production rates suggested by West et al., as in the case of hydrazine, require that

99% of the P_2H_4 produced be removed by the condensational growth of large (>10 μm) particles and subsequent sedimentation. Whether or not such large particles can be produced depends strongly on the thermodynamic properties of P_2H_4 which control the condensation process; but in any case the removal rate of 10 μm particles is not high enough to make them unobservable.

Our investigation of other detected or proposed species indicates that many of the photochemically-produced hydrocarbons [e.g., acetylene (C_2H_2), ethane (C_2H_6), ethylene (C_2H_4), and propane (C_3H_8)] may condense in the atmospheres of Uranus and Neptune (cf. Pollack et al. 1987). Other hydrocarbons may condense but vapor pressure/thermodynamic data are unavailable for them at this time (Pollack et al. 1987 include C_4H_2). Fig. 10 shows the variation of the saturation mixing ratios of several hydrocarbons with temperature for the atmosphere of Uranus. Since the hydrocarbons are probably produced by methane photolysis, an upper limit on their abundance is simply the methane abundance at the tropopause level, 10^{-5}. (This value is based on saturation and therefore independent of the methane abundance at depth provided that it is larger than 10^{-5}). From Fig. 10, one can see that even if the abundances of these compounds are only of order 10^{-9}, a photochemical hydrocarbon haze layer is expected to extend downward from ~0.01 bar through the temperature minimum (Pollack et al. 1987, obtain aerosol from 0.0001 bar downward). Of the hydrocarbons investigated only propane may remain saturated throughout the CH_4 cloud region. Even if the abundances of some of the compounds are $\gg 10^{-9}$, their low saturation vapor pressures insure that their vapor mixing ratios will remain at or below the current levels of detectability.

Assuming that the abundances are of order 10^{-9}, a conservative estimate, the vertical column density of aerosol is $\sim 10^8$ cm^{-2}. Thus the aerosol layer is comparable to that observed on Jupiter in terms of the vertical column density (West et al. 1986). If, however, the actual hydrocarbon abundances are closer to the Jovian values, then column densities of order 10^{10} cm^{-2} are expected. (For reference, the vertical column density of stratospheric aerosol on Saturn is 10^9 cm^{-2} based on West et al. 1983). The particle sizes would typically be submicron, although near the base of the stratosphere, micron-sized particles are expected. Thus, it is likely that there are several overlapping layers of optically significant aerosol extending from 0.001 to 0.01 bar down to the top of the tropospheric CH_4 cloud layer (Pollack et al. 1987 provide a more detailed model fit to *Voyager* observations with several aerosol layers).

As in the case of methane on Uranus and Neptune and acetylene on Saturn, the presence of clouds adds greater uncertainty to the abundances determined by remote sensing. The mixing ratio of a condensate determined from a gas phase feature depends strongly on the pressure level sensed (i.e., above or below the cloud). If the abundance is determined from the above cloud region, the measured value represents a lower limit; for some of these species at very low vapor pressures, large supersaturations may be maintained by the photochemical production. Also, since the vapor *mixing ratio* of a condensing species decreases rapidly above the cloud base, measurements based on "relatively weak" absorption lines must look "through" much of the cloud to see enough absorption; improper handling of the vapor profile in this region can produce misleading results. Neglect of aerosol opacity in the analysis at some wavelengths can also lead to important errors. Further observations and modeling of cloud vertical structures may be required to unscramble these complicated, layered atmospheres.

4. Discussion

The results of theoretical thermochemical equilibrium (cf. Carlson et al. 1987a,b) and cloud microphysical studies can provide an interesting context in which to interpret planetary observations. Thermochemical equilibrium studies are capable of providing some useful constraints on the composition, potential structure and chemical complexity of the clouds, as well as the condensate abundance. Although these models do not include the effects of dynamics, they do provide some information on the cloud layers possible within these planetary atmospheres. As indicated by the results in Figs. 2, 3 and 4 and Table 4, the actual locations are still somewhat uncertain because of uncertainties in the thermal structure of these atmospheres and condensate abundances. As the *Voyager* IRIS results have shown for Jupiter and Saturn (Pirraglia et al. 1981), the temperature profile is latitudinally dependent. There are also indications that condensate abundances are latitudinally dependent (Hanel et al. 1979; Courtin 1982; Drossart and Encrenaz 1982). Furthermore, the temperature profiles (Caldwell et al. 1979; Carlson et al. 1980; Bezard and Gautier 1985) and condensate abundances are also temporally variable (Drossart et al. 1984).

a. Cloud system analogs

Despite these uncertainties, many of the tropospheric clouds we have examined can still be characterized as having microphysical balances similar to water clouds in Earth's lower troposphere: the NH_3 clouds on Uranus and Neptune and the H_2O clouds on Jupiter and Saturn. The NH_3 clouds on Jupiter and Saturn are more like dense cirrus and thin stratus, respectively. The NH_4SH clouds are tenuous on Jupiter and Saturn, but may form precipitation on Uranus and Neptune, if sticking of the solid particles is possible. The CH_4 and H_2O clouds on Uranus and Neptune are unlike clouds on Earth, being 10–100 times as massive.

The rapid formation of precipitation can have two consequences: significant latent heat feedback on dynamics and "drying" of downdrafts. Those systems with large mass densities, >1 g m^{-3}, are expected to exhibit significant horizontal and vertical structure controlled by dynamics, but influenced by latent heat feedbacks similar to deep convective clouds on Earth. This situation makes cumulus-style dynamics more likely than stratus dynamics in the CH_4 and H_2O clouds. In contrast, NH_3 clouds on Jupiter and Saturn are less dense than lower tropospheric H_2O clouds, but similar to cirrus on Earth, and only weakly precipitating. Consequently, horizontal contrasts may be muted and vertical extent may be small in a weak dynamic regime. However, in a weak dynamic regime interactions between radiation, dynamics, and microphysics become important and can lead to complex, multiple layer hazes (cf. Curry 1986) as occurs in the Arctic. On Uranus and Neptune, where the NH_3 clouds are denser and more strongly precipitating, there may be more horizontal variations of cloud properties.

Solar abundance H_2O clouds on Jupiter are denser than H_2O clouds on Earth and are expected to exhibit more spatial variation than NH_3 clouds, with a stronger feedback on dynamics due to the latent heat effects. H_2O clouds on Uranus and Neptune reach conditions unlike anything on Earth, where the droplet size distribution reaches complete collisional equilibrium, even in very weak updrafts. The consequences of these massive H_2O clouds for the general circulation are likely to be significant and complex.

The stratospheric clouds examined here are representative of the types of clouds possible given the chemical compositions of the giant planets. These clouds can typically be regarded as hazes because of their low mass densities. None of these systems are massive enough to produce precipitation.

b. *Vertical structure*

The vertical structure of these cloud layers cannot be predicted without a consideration of dynamics; however, analogies to similar Earth systems can suggest some possibilities. Low density clouds, such as the NH_3 and NH_4SH clouds on Jupiter and Saturn, are characterized by slow growth processes which, in turn, can produce only moderate sized particles ($\sim$10–100 μm) before sedimentation removes them. If sticking efficiencies are low, as likely for solid particles, particle sizes will be at the lower end of this range.

Gierasch et al. (1986) used the particle optical depths at 45 and 5 μm inferred from the *Voyager* IRIS data to constrain the sizes of NH_3 ice particles in the atmosphere of Jupiter to be of the order 6 μm. Note however, that particle sizes inferred from remote sensing observations can be considered to be cross section weighted mean values; for typical size distributions these sizes would be a factor of 1.5 to 2 smaller than the mass-weighted mean values we use. A more recent analysis by Shaffer and Samuelson (1987) fitted particle optical depths at 45 and 8.6 μm and, including constraints on the suppression of resonant absorption features in the spectrum, derived particle sizes in either of two ranges, 1.25 or 2.9 μm. Thus, although both studies derived results from the same dataset, different spectral regions were used, with a "consensus" being in the approximate range of 3 μm. Sustained updraft velocities < 1 m s^{-1} will have little effect on these clouds because the sedimentation velocity of 10 μm sized particles is already 1 m s^{-1} and increases as the square of the particle radius [see Eq. (11)]. Only very much stronger updrafts can alter the mean particle size attained in these clouds.

Therefore, these low mass clouds, by analogy to upper tropospheric cirrus clouds or Arctic stratus, will exhibit a vertical variation of particle size that is governed by the region over which upward motions cause condensation. In a weak circulation regime, these updrafts can be influenced by the radiation perturbation caused by the clouds (see Curry 1986 for references for Arctic and marine stratus clouds; see Starr 1987 for references for cirrus clouds). Since the sedimentation rate and condensation rate are relatively independent of pressure and temperature (for small particles, <10 μm, and pressures > 0.1 bar), the only factor influencing particle size is the dynamic control of S_{max}: weaker updrafts tend to produce fewer and smaller particles; however, mixing processes in clouds produce much more complex altitude variations (e.g., Paluch 1986). Since vapor scavenging by precipitation is insignificant, vapor pressures are expected to remain near saturation unless horizontal mixing of different temperature air masses occurs. In this case multiple haze-like layers can occur.

Higher mass density clouds exhibit very rapid growth of precipitation-sized particles, before sedimentation removal occurs. CH_4 ice may exhibit significant sticking, since it forms near its freezing temperature, whereas NH_3 and NH_4SH do not. Collisional disruption limits sizes in the liquid H_2O clouds, but may not limit particle size in the CH_4 clouds. Strong updrafts probably cannot affect this balance directly, but rather they influence the rate of vapor supply that balances the rapid scavenging of the condensate by the precipitation. Significant latent heat effects imply the possibility on Earth for strong, but small-scale, motions with large precipitation rates; however, strong large-scale updrafts can also sustain persistent heavy precipitation. The key relationship, that microphysical times are much shorter than dynamical times, implies that "typical" conditions cannot supply vapor to cloud level as rapidly as it is converted to precipitation. Thus, the cloud mass density must be smaller "typically" and ascending air dried effectively, producing larger horizontal contrasts in cloud properties. Weakly precipitating systems (NH_3 on Jupiter/Saturn) should not ex-

hibit as large humidity and cloud density contrasts as the strongly precipitating systems (NH_3 on Uranus/Neptune and H_2O on all of the planets).

The rapid depletion by precipitation of the condensate in an ascending parcel does not preclude vertically extensive layers of cloud, since horizontal dynamical mixing can lead to multiple layers. Rapid condensation growth, compared to dynamic transport times, precludes supersaturated vapor pressures. However, as the mass density of a cloud decreases strongly with altitude (*mass mixing ratio* declines *exponentially*, following saturation profile), precipitation is no longer formed in the upper level clouds as coalescence is no longer effective. Without precipitation to act as a strong drying process, even weak dynamic transports will eventually raise the vapor pressure to near-saturated levels. Hence, under the proper dynamical conditions other cloud layers can form well above the main thermodynamic layer. Analogy with Earth H_2O clouds suggests, however, that predicting the properties or even the existence of these upper hazes is difficult without knowledge of the atmospheric circulation: a general theory of upper tropospheric cloudiness on Earth does not exist (cf. Starr 1987). The key point is that none of these condensible species can be assumed to be neatly confined in a single, well-specified cloud layer. The classical picture of three or four, compositionally distinct cloud layers on Jupiter (or any other giant planet) may not be accurate.

c. *Scavenging and chemistry*

The rapid cycling of condensible substances in the precipitating clouds, together with the formation of large particles that may fall as much as a scale height before evaporating, has possible consequences on the vertical distribution of other aerosols and any gases which can react with the condensed phase. In particular, the dense H_2O clouds likely to be present in all of these atmospheres may serve as strong filters of some chemical species mixed up from deeper levels (Carlson et al. 1987a). Efficient scavenging of substances by condensing H_2O would also suggest that a large vertical gradient in these substances would be maintained in the vicinity of the lowest H_2O cloud layer. The steep vertical gradient in the NH_3 mixing ratio observed in these atmospheres, combined with the observational constraints on the H_2S abundance, leads one to suspect the formation of an NH_4SH condensate. From a microphysical standpoint the NH_4SH clouds are intermediate in nature, having mass densities and precipitation rates between the NH_3 and H_2O cloud values.

Acknowledgments. We thank D. Linder for performing some of the calculations used in this paper. We are grateful to Drs. M. J. Prather and J. F. Appleby for many helpful discussions. We thank D. Purdy and L. Lawton for their assistance in obtaining reference material and L. Del Valle for preparing the figures. G.O. acknowledges support of NASA Office of Space Science Application, Planetary Atmospheres Discipline through grants to the Jet Propulsion Laboratory, California Institute of Technology.

REFERENCES

Allison, M., and L. D. Travis, 1986: Astronomical, physical and meteorological parameters for planetary atmospheres. *Atmospheres of the Jovian Planets,* M. Allison and L. Travis, Eds., NASA CP-2441, 293–319.

Appleby, J. F., 1986: Radiative-convective equilibrium models for Uranus and Neptune. *Icarus,* **65,** 383–405.

Atreya, S. K., T. M. Donahue and W. R. Kuhn, 1977: The distribution of ammonia and its photochemical products on Jupiter. *Icarus,* **31,** 348–355.

Bergstralh, J. T., and J. S. Neff, 1983: Absolute spectrophotometry of Neptune: 3390–7800 Å. *Icarus,* **55,** 40–49.

——, and K. H. Baines, 1984: Properties of the upper troposphere of Uranus and Neptune derived from observations at "visible" to near-infrared wavelengths. *Uranus and Neptune* J. T. Bergstralh, Ed., NASA CP-2330, 179–206.

Bezanger, C., B. Bezard and D. Gautier, 1986: Spatial variation of the thermal structure of Jupiter's atmosphere. *Atmospheres of the Jovian Planets* M. Allison and L. Travis, Eds., NASA CP 2441, 79–82.

Bezard, B., and D. Gautier, 1985: A seasonal climate model of the atmospheres of the giant planets at the Voyager encounter time I. Saturn's seasonal stratosphere. *Icarus,* **61,** 296–310.

——, A. Marten, J. P. Baluteau, D. Gautier, J. M. Flaud and C. Camy-Peyret, 1983b: On the detectability of H_2S on Jupiter. *Icarus,* **55,** 259–271.

Bjoraker, G. L., H. P. Larson and V. G. Kunde, 1986: The abundance and distribution of water vapor in Jupiter's atmosphere. *Astrophys. J.,* **311,** 1058–1072.

Caldwell, J., 1977: Ultraviolet observations of Mars and Saturn by the TD1A and by the OAO-2 satellites. *Icarus,* **32,** 190–209.

——, R. D. Cess, B. E. Carlson, A. T. Tokunaga, F. C. Gillett and I. G. Nolt, 1979: Temporal characteristics of the Jovian atmosphere. *Astrophys. J.,* **234,** L155–L158.

Cameron, A. G. W., 1982: Elementary and nuclideo abundances in the solar system. *Essays in Nuclear Astrophysics* C. A. Barnes, D. D. Clayton and D. N. Schramm, Eds. Cambridge University Press, 23–43.

Carlson, B. E., J. Caldwell and R. D. Cess, 1980: A model of Saturn's seasonal stratosphere at the time of the Voyager encounters. *J. Atmos. Sci.,* **37,** 1883–1885.

——, M. J. Prather and W. B. Rossow, 1987a: Cloud chemistry on Jupiter. *Astrophys. J.,* **322,** 559–572.

——, —— and ——, 1987b: The role of aqueous chemistry in determining the composition and cloud structure of the upper troposphere on Uranus. *Astrophys. J.,* **321,** L97–L101.

Conrath, B. J., F. M. Flasar, J. A. Pirraglia, P. J. Gierasch and G. E. Hunt, 1981: Thermal structure and dynamics of the Jovian atmosphere. 2. Visible cloud features. *J. Geophys. Res.,* **86,** 8769–8775.

——, D. Gautier, R. A. Hanel and J. S. Hornstein, 1984: The helium abundance of Saturn from Voyager measurements. *Astrophys. J.,* **282,** 807–815.

Courtin, R., 1982: *La structure thermique et la composition des atmospheres des planetes geantes a partir de leur spectra infrarouge lointain.* thesis, Paris University.

——, D. Gautier, A. Marten and B. Bezard, 1984: The composition of Saturn's atmosphere at northern temperate latitudes from Voyager IRIS spectra: NH_3, PH_3, C_2H_2, C_2H_6, CH_3D, CH_4, and the Saturnian D/H ratio. *Astrophys. J.,* **287,** 899–916.

Curry, J. A., 1986: Interactions among turbulence, radiation and microphysics in Arctic stratus clouds. *J. Atmos. Sci.,* **43,** 90–106.

Drossart, P., and T. Encrenaz, 1982: The abundance of water on Jupiter from Voyager IRIS data at 5 μm. *Icarus*, **52**, 483–491.

——, —— and A. T. Tokunaga, 1984: Variability of phosphine on Jupiter from 5 μm spectroscopy. *Icarus*, **60**, 613–620.

Flasar, F. M., B. J. Conrath, P. J. Gierasch and J. A. Pirraglia, 1987: Voyager infrared observations of Uranus' atmosphere: Thermal structure and dynamics. *J. Geophys. Res.*, **92**, 15 011–15 018.

Gautier, D., B. Bezard, A. Marten, J. P. Baluteau, N. Scott, A. Chedin, V. Kunde and R. Hanel, 1981: The C/H ratio in Jupiter from the Voyager infrared investigation. *Astrophys. J.*, **257**, 901–912.

——, B. Conrath, M. Flasar, R. Hanel, V. Kunde, A. Chedin and N. Scott, 1981: The helium abundance of Jupiter from Voyager. *J. Geophys. Res.*, **86**, 8713–8720.

Giaque, W. F., and R. W. Blue, 1936: Hydrogen sulfide. The heat capacity and vapor pressure of solid and liquid. The heat of vaporization. A comparison of thermodynamic and spectroscopic values of the entropy. *J. Amer. Chem. Soc.*, **58**, 831–837.

Gierasch, P. J., B. J. Conrath and J. A. Magalhaes, 1986: Zonal mean properties of Jupiter's upper troposphere from Voyager. *Icarus*, **67**, 456–483.

Handbook of Chemistry and Physics, 1983: Chemical Rubber Publ. Co.

Hanel, R., B. Conrath, M. Flasar, L. Herath, V. Kunde, P. Lowman, W. Maguire, J. Pearl, J. Pirraglia, R. Samuelson, D. Gautier, P. Gierasch, L. Horn, S. Kumar and C. Ponnamperuma, 1979: Infrared observations of the Jovian system from Voyager 2. *Science*, **206**, 952–956.

——, ——, ——, V. Kunde, W. Maguire, J. Pearl, J. Pirraglia, R. Samuelson, L. Herath, M. Allison, D. Cruikshank, D. Gautier, P. Gierasch, L. Horn, R. Koppany and C. Ponnamperuma, 1981: Infrared observations of the Saturnian system from Voyager 1. *Science*, **212**, 192–200.

International Critical Tables, 1928: McGraw-Hill Book Co., Inc.

JANAF Thermochemical Tables, 1971: Second ed. D. R. Stull and H. Prophet project directors. NSRDS-NBS37. U.S. Govt. Print. Off. Washington, D.C.

Kelley, K. K., 1962: *Contributions to the data on Theoretical Metallurgy XV. A reprint of bulletins 303, 384, 393 and 406.* U.S. Govt. Print. Off. Washington, 44–115.

——, and E. G. King, 1961: *Contributions to the data on Theoretical Metallurgy XIV. Entropies of the elements and inorganic compounds.* U.S. Govt. Print. Off. Washington, D.C. 23–118.

Kunde, V., R. Hanel, W. Maguire, D. Gautier, J. P. Baluteau, A. Marten, A. Chedin, N. Husson and N. Scott, 1982: The tropospheric gas composition of Jupiter's North Equatorial Belt (NH_3, PH_3, CH_3D, GeH_4, H_2O) and the Jovian D/H ratio. *Astrophys. J.*, **263**, 443–467.

Lewis, J. S., 1969: The clouds of Jupiter and the NH_3–H_2O and NH_3–H_2S systems. *Icarus*, **10**, 365–378.

Lindal, G. F., G. E. Wood, G. S. Levy, J. D. Anderson, D. N. Sweetnam, H. B. Hotz, B. J. Buckles, D. P. Holmes, P. E. Doms, V. R. Eshleman, G. L. Tyler and T. A. Croft, 1981: The atmosphere of Jupiter: An analysis of the Voyager radio occultation measurements. *J. Geophys. Res.*, **86**, 8721–8727.

——, D. N. Sweetnam and V. R. Eshleman, 1985: The atmosphere of Saturn: An analysis of the *Voyager* Radio Occultation measurements. *Astron. J.*, **90**, 1136–1146.

——, J. R. Lyons, D. N. Sweetnam, V. R. Eshleman, D. P. Hinson, and G. L. Tyler, 1987: The atmosphere of Uranus: Results of radio occultation measurements with Voyager 2. *J. Geophys. Res.* **92**, 14 987–15 001.

McCormick, M. P., H. M. Steele, P. Hamill, W. P. Chu and T. J. Swissler, 1982: Polar stratospheric cloud sightings by SAM II. *J. Atmos. Sci.*, **39**, 1387–1397.

Orton, G. S., 1981: Atmospheric structure in the equatorial region of Jupiter: A report of the Galileo Working Group on Atmospheres, Subcommittee on Atmospheric Structure. Galileo Document No. 1625-125.

——, M. J. Griffin, P. A. R. Ade, I. G. Nolt, J. V. Radostitz, E. I. Robson and W. K. Gear, 1986: Submillimeter and millimeter observations of Uranus and Neptune. *Icarus*, **67**, 289–304.

Paluch, I. R., 1986: Mixing and the cloud droplet size spectrum: Generalizations from the CCOPE data. *J. Atmos. Sci.*, **43**, 1984–1993.

de Pater, I., 1986: Jupiter's zone-belt structure at radio wavelengths. *Icarus*, **68**, 344–365.

——, and S. T. Massie, 1985: Models of millimeter–centimeter spectra of the giant planets. *Icarus*, **62**, 143–171.

Pirraglia, J. A., B. J. Conrath, M. Allison and P. Gierasch, 1981: Thermal structure and dynamics of Saturn and Jupiter. *Nature*, **292**, 677–679.

Pollack, J. B., K. Rages, S. K. Pope, M. G. Tomasko, P. N. Romani and S. K. Atreya, 1987: Nature of the stratospheric haze on Uranus: Evidence for condensed hydrocarbons. *J. Geophys. Res.*, **92**, 15 037–15 065.

Prinn, R. G., H. P. Larson, J. J. Caldwell and D. Gautier, 1983: Composition and chemistry of Saturn's atmosphere. *Saturn* T. Gehrels and M. S. Matthews, Eds., University of Arizona Press, 88–149.

Rossow, W. B., 1978: Cloud microphysics: Analysis of the clouds of Earth, Venus, Mars and Jupiter. *Icarus*, **36**, 1–50.

Sato, M. and J. E. Hansen, 1979: Jupiter's atmospheric composition and cloud structure deduced from absorption bands in reflected sunlight. *J. Atmos. Sci.*, **36**, 1133–1167.

Scott, D. W., G. D. Oliver, M. E. Gross, W. N. Hubbard and H. M. Huffman, 1949: Hydrazine: Heat capacity, heats of fusion and vaporization, vapor pressure, entropy and thermodynamic functions. *J. Amer. Chem. Soc.*, **71**, 2293–2297.

Shaffer, W., and R. Samuelson, 1987: Study of the NH_3 cloud in Jupiter's North Tropical Zone. *Bull. Amer. Astron. Soc.*, **19**, 632.

Starr, D. O'C., 1987: A cirrus-cloud experiment: Intensive field observations planned for FIRE. *Bull. Amer. Meteor. Soc.*, **68**, 119–124.

Stobel, D. F., 1973: The photochemistry of NH_3 in the Jovian atmosphere. *J. Atmos. Sci.*, **30**, 1205–1209.

Tomasko, M. G., and L. R. Doose, 1984: Polarimetry and photometry of Saturn from Pioneer 11: Observations and constraints on the distribution and properties of cloud and aerosol particles. *Icarus*, **58**, 1–34.

Tyler, G. L., D. N. Sweetnam, J. D. Anderson, J. K. Campbell, V. R. Eshleman, D. P. Hinson, G. S. Levy, G. F. Lindal, E. A. Marouf and R. A. Simpson, 1986: Voyager 2 radio science observations of the Uranian system: Atmospheres, rings and satellites. *Science*, **233**, 79–84.

Wagener, R., J. Caldwell, T. Owen, S. J. Kim, T. Encrenaz and M. Combes, 1985: The Jovian stratosphere in the ultraviolet. *Icarus*, **63**, 222–236.

Wagman, D. D., W. H. Evans, V. B. Parker, I. Halow, S. M. Baily and R. H. Schumm, 1968: NBS Technical Note 270-3. U.S. Govt. Printing Office Washington, DC.

Wallace, L., 1984: The seasonal variation of the thermal structure of the atmosphere of Uranus. *Icarus*, **54**, 110–132.

Weidenschilling, S. J., and J. S. Lewis, 1973: Atmospheric and cloud structures of the Jovian planets. *Icarus*, **20**, 465–476.

West, R. A., M. Sato, H. Hart, A. L. Lane, C. H. Hord, K. E. Simmons, L. W. Esposito, D. L. Coffeen and R. B. Pomphrey, 1983: Photometry and polarimetry of Saturn at 2640 and 7500. *J. Geophys. Res.*, **88**, 8679–8698.

——, D. F. Strobel and M. G. Tomasko, 1986: Clouds aerosols and photochemistry in the Jovian atmosphere. *Icarus*, **65**, 161–217.

Ziegler, W. T., 1959: The vapor pressure of some hydrocarbons in liquid and solid state at low temperatures. National Bureau of Standards Tech. Note No. 4 (PB 151363).